Ultrasonic Characterization of Silt Suspensions by Backscattering

Peter Fleckenstein*, Fabian Deschwanden†, Giuseppe Storti*, Marco Lattuada‡, Peter Gruber†
* Institute for Chemical- and Bioengineering, ETH Zürich, Zürich, Switzerland
‡ Adolph Merkle Institute, Fribourg, Switzerland
† Hochschule Luzern, Luzern, Switzerland

Several models for the scattering of sound waves by spherical particles were comparatively investigated. The models included both rigorous approaches like the ones suggested by Faran, Epstein-Carhart-Allegra-Hawley, Hay and Mercier as well as semiempirical approaches by Kytömaa, Moore and Skripalle. It was found, that Farans model is numerically more stable than the other rigorous approaches while providing sufficient detail. This makes it superior to the semiempirical models, which are numerically easy to handle, but fail to describe scattering for larger particle sizes and frequencies.

Keywords: Acoustical Characterization, Mathematical Modeling, Silt Suspensions, Backscattering.

1 INTRODUCTION

Ultrasound scattering is a physical phenomenon of considerable importance for many applications. Amongst them are particle sizing [1] , zeta-potential measurements and diagnostic applications in several medical disciplines [2]. Such a huge spectrum of applications justifies the plethora of modeling approaches developed to describe this phenomenon.

Aimed to select the optimal model for particle sizing by sound backscattering, in this work we focus on modeling approaches developed to describe the behavior of spherical objects. The approaches are divided into two groups. The first group includes models based on the two phase approach, such as the one developed by Kytömaa and Atkinson [3–6]. This model is capable to provide accurate relationships for the attenuation and sound speed in a suspension, as long as the particles are not large compared to the sound wavelengths. However it cannot be used to describe backscattering since the propagation and attenuation of sound waves is only considered in the forward direction.

The second group of models considers the scattering behavior of individual particles by solving the equation of wave propagation inside and outside the particles [7]. They can cover single scattering as well as multiple scattering [8] (which is extremely challenging). This group of models includes those developed by Faran [9], Epstein-Carhart-Allegra-Hawley (ECAH) [10,11] and Hay and Mercer (HM) [12]. The advantage of these models is the accurate description of the scattering behavior of particles combined with the possibility to include elastic, viscous and thermal effects simultaneously. The three approaches differ only in the underlying approximations and will be now discussed in more detail.

2 RIGOROUS MODELS

2.1 Faran Model

Faran model for the scattering of sound waves by spherical particles is based on three main assumptions: (i) the mechanical behavior of the particle follows classical continuous mechanics for elastic objects, (ii) the continuous phase is considered inviscid, and (iii) thermal dissipation is neglected. Additional assumptions are plane incident sound wave, steady state irradiation and wavelength larger than the particle size. The displacement of a sphere by an acoustical wave can then be derived from a scalar potential, ψ and a vector potential A [9].

$$u = -\nabla\psi + \nabla\times\mathbf{A} \tag{1}$$

The displacement can be separated into the two wave equations:

$$\nabla^2\psi = \frac{1}{c_1^2}\frac{\partial^2\psi}{\partial t^2} \tag{2}$$

$$\nabla^2\mathbf{A} = \frac{1}{c_2^2}\frac{\partial^2\mathbf{A}}{\partial t^2} \tag{3}$$

Equations (2) and (3) describe the propagation of longitudinal and shear waves respectively. The solution of these equations requires the specification of three boundary conditions at the particle interface: (i) the pressure of the fluid and normal stress are equal, (ii) the displacement of fluid and solid is equal, and (iii) the tangential and shear stresses are zero. The relationship between displacement and pressure is given by [9]:

$$u_r = \frac{1}{\rho_3\omega^2}\frac{\partial p_i}{\partial r} \tag{4}$$

Accordingly, the scattered pressure becomes:

$$p_s = p_i \sum_{n=0}^{\infty} (2n+1)(-1)^n \sin(\eta_n)\exp(-i\eta_n) h_n(k_c r) P_n(\cos\theta) \quad (5)$$

where p_i is the incident pressure θ is the scattering angle and h_n is the hyperbolic Bessel function. The so called phase shift of the n^{th} scattered wave η_n is defined as:

$$\tan\eta_n = \tan(\delta_n(x_3)) \frac{\tan\Phi_n + \tan(\alpha_n(x_3))}{\tan\Phi_n + \tan(\beta_n(x_3))} \quad (6)$$

with the intermediate angles given by:

$$\begin{aligned} \delta_n(x_i) &= \tan^{-1}\left(\frac{-j_n(x_i)}{n_n(x_i)}\right) \\ \alpha_n(x_i) &= \tan^{-1}\left(\frac{x j_n'(x_i)}{j_n(x_i)}\right) \\ \beta_n(x_i) &= \tan^{-1}\left(\frac{n_n'(x_i)}{n_n(x_i)}\right) \end{aligned} \quad (7)$$

The boundary impedance phase angle is equal to:

$$\tan\Phi_n = -\frac{\rho_3}{\rho_1}\tan\zeta_n(x_1, x_2, x_3, \sigma) \quad (8)$$

where the function ζ_n is easy to implement and numerically stable [9]. Furthermore it only depends on three physical parameters of the solid: the density ρ_1, the compressional velocity c_1 and the Poisson ratio σ. The last two quantities are involved in the expressions of x_i as follows:

$$\begin{aligned} x_1 &= k_1 a = \frac{\omega}{c_1} a \\ x_2 &= k_2 a = \frac{\omega}{c_2} a \\ x_3 &= k_c a = \frac{\omega}{c} a \end{aligned} \quad (9)$$

where c_2 is the shear velocity, which is given as a function of c_1 and σ

$$c_2 = \sqrt{\frac{3c_1^2(1-2\sigma)}{2(3-5\sigma)}}\,. \quad (10)$$

Far Field Function

The far field function is defined as an approximation of the amplitude of a scattered wave at large distance from the particle:

$$f_\infty = \frac{2r}{a}\frac{p_s}{p_i} \quad (11)$$

Equation (5), the equation for the pressure, can be simplified at large distances from the sphere as follows:

$$\lim_{r\to\infty} |\, p_s \,| = \frac{p_i}{k_c r}\left|\sum_{n=0}^{\infty} i(2n+1)\sin(\eta_n)\exp(-i\eta_n) P_n(\cos\theta)\right| \quad (12)$$

leading to the following expression for the far field function for the Faran model:

$$f_\infty = -\frac{2}{x_3}\sum_{n=0}^{\infty} i(2n+1)\sin(\eta_n)\exp(-i\eta_n) P_n(\cos\theta) \quad (13)$$

Attenuation

The attenuation coefficient α_s describes the loss of acoustic energy over a distance $\Delta z = z_1 - z_2$, and can be expressed as:

$$\alpha_s = \frac{1}{\Delta z}\ln\frac{p|_{z_1}}{p|_{z_2}} \quad (14)$$

An expression for the attenuation for the ECAH model [10,11] can be found in the Doctoral thesis of Hipp [7]. Using similarities in the ECAH and Faran models, the following expression for the attenuation in the Faran model was found:

$$\alpha_s = \frac{-3}{2(k_c a)^2 a}\sum_{n=0}^{\infty}(2n+1)\Re e\{-i\cdot\sin(\eta_n)\exp(-i\eta_n)\} \quad (15)$$

Note that the attenuation has to be multiplied by the volume fraction of particles and added to the attenuation of the dispersed phase.

2.2 The ECAH model

The ECAH model is the most accurate and comprehensive approach developed to account for sound scattering by particles[10]. The assumption of isotropicity and linear elastic behavior of particles is extended by suitable expressions for viscous and thermal dissipations. This comes at the cost of a more complex theoretical description of the problem, and ill-conditioned equations. Nevertheless this model represents a gold standard, against which all other approaches need to be tested. The relevant equations of the model, and the articulated boundary conditions, are reported in the abundant literature on the topic [10,11].

2.3 The HM model

The model proposed by Hay and Mercer [12] is an intermediate between Faran and ECAH. Thermal effects are neglected leading to equations a bit simpler and less accurate than ECAH. Numerically speaking, the HM model is slightly more robust and less ill-conditioned than the ECAH, but still very challenging. Once more, the corresponding equations (fully available in the original paper) are omitted.

2.4 Model comparison (Faran, ECAH, HM)

A comparison among the three models was carried out in the case of monodisperse spherical particles made of silica with radius a = 50 μm, over a broad range of frequencies.

Figure 1 shows the far-field function computed through the models by Faran, ECAH and HM. At

very low frequency the ECAH and HM models are always identical and show little deviation from Faran model. This proves that thermal effects are negligible and viscous effects have little effect on the far-field function, which is rather dominated by elastic scattering effects. At higher frequencies, it is seen that ECAH model is not able to provide any result, while the HM model shows some deviations from Faran model predictions. Both effects are due to numerical issues.

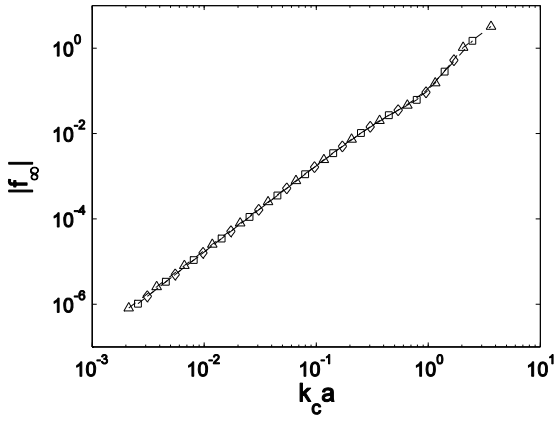

Figure 1 Comparison of the far field functions for 3 different models: Faran (Δ), HM (□), ECAH (◊).

Figure 2 shows the predictions of the three models for the attenuation, computed in the case of a particle volume fraction of 1%. For sufficiently high $k_c \cdot a$ values the three models provide identical results. This indicates the dominant role played by the scattering contribution. At low $k_c \cdot a$ values, Faran model greatly underestimates the attenuation values. This is caused by neglecting the viscous contributions. The attenuation provided by Kytömaa was added to the figure, which greatly underestimates the attenuation for large particle sizes.

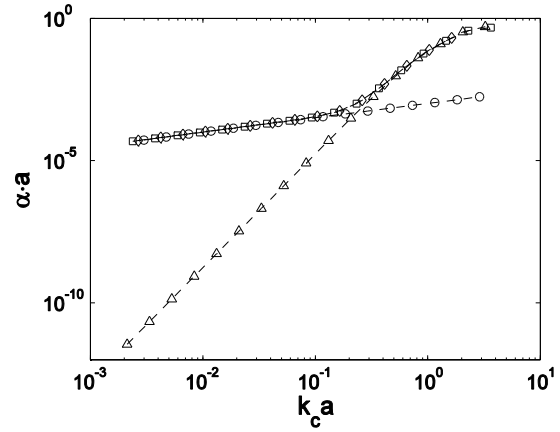

Figure 2 Comparison of attenuation for 4 different models: Faran (Δ), HM (□), ECAH (◊), Kytömaa (○).

Based on these results, we can conclude that Faran model is suitable to describe the far-field function, which is essential to compute the backscattering, in the entire regime of interest. In the case of attenuation, however, Faran model is only suitable for sufficiently large particles, while the predictions of Kytömaa model could be superimposed to correct such lack.

3 SEMIEMPIRICAL MODELS

3.1 Moore model [13]

Semiempirical expressions for f_∞ and α_s were provided in the Doctoral Thesis of Moore. These functions were obtained by comparison with experimental data. The only parameter entering the equation for the far field function is $x=k_c \cdot a$. The far field function is given by the following expression:

$$f_\infty = \frac{x^2\left(1-0.35\exp(-((x-1.5)/0.7)^2)\right)\left(1+0.5\exp(-((x-1.8)/2.2)^2)\right)}{1+0.9x^2} \quad (16)$$

while the attenuation for the scatterers is given as summation of the viscous attenuation and the attenuation due to scattering:

$$\alpha_s = \alpha_{s,visc} + \alpha_{s,scat} = M\zeta_v + M\zeta_s \quad (17)$$

where M is the mass concentration of the scatterers and ζ_v and ζ_s are expressed as:

$$\zeta_v = \frac{k(g-1)^2}{2\rho_s}\left[\frac{s}{s^2+(g+\delta)^2}\right] \quad (18)$$
$$s = \frac{9}{4ba}\left[1+\frac{1}{ba}\right]$$
$$g = \frac{\rho_s}{\rho},\ \delta = \frac{1}{2}\left[1+\frac{9}{2ba}\right],\ b = \sqrt{\frac{\omega}{2\nu}}$$

$$\zeta_s = \frac{3\chi}{4\rho_s a} \quad (19)$$
$$\chi = \frac{0.29x^4}{0.95+1.28x^2+0.25x^4}$$

where ν is the kinematic viscosity and ρ_s and ρ are the densities of scatterers and medium, respectively.

3.2 Skripalle model [14]

Semiempirical equations similar to those proposed by Moore were provided in the work of Skripalle et al.. The far field function is expressed in this case by the following equation:

$$f_\infty = \frac{1.21x^2\left(1-0.25\exp(-((x-1.4)/0.5)^2)\right)\left(1+0.37\exp(-((x-2.8)/2.2)^2)\right)}{1+1.1x^2} \quad (20)$$

while the attenuation is given by Equations (17), (18) and (19), with the function χ expressed by:

$$\chi = \frac{0.264x^4}{1+1.3x^2+0.24x^4} \quad (21).$$

3.3 Model comparison (Faran, Moore, Skripalle)

The far field functions computed through equation (13) (Faran), equation (16) (Moore) and equation (20) (Skripalle) are compared in Figure 3. One should note that Faran model predicts an angular dependence for the far field function, while the curve in Figure 3 only refers to the case of direct backscattering. The models agree very well for sufficiently small $k_c \cdot a$ values. On the other hand, when $k_c \cdot a$ increases, the semiempirical models seem to reach an asymptotic value, while Faran model displays strong oscillations.

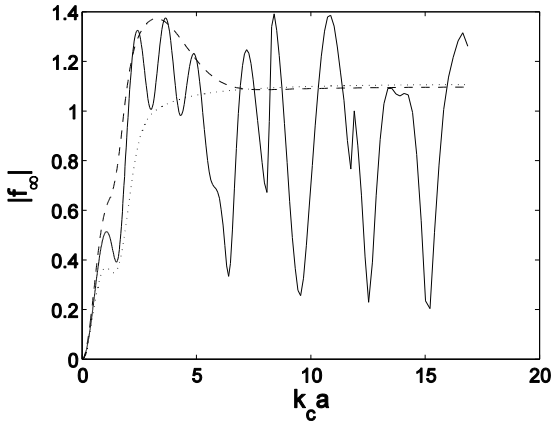

Figure 3 Comparison of the far field functions for 3 different models: Faran (-), Moore (..), Skripalle (--).

Figure 4 shows instead a comparison of a normalized attenuation $\alpha_s \cdot a$ as a function of the variable $x=k_c \cdot a$. One can observe that all models predict once more the same behavior for small values of x, where the dimensionless attenuation scales as x^4. On the other hand, as soon as $k_c \cdot a$ increases Faran model shows strong deviations, as well as oscillatory behavior. Considering far field function and attenuation it can be seen, that the two empirical models are only valid in a narrow range of $k_c \cdot a$ values.

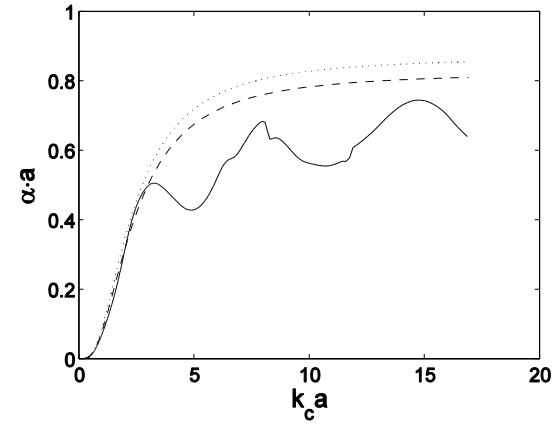

Figure 4 Comparison of the attenuation for 3 different models: Faran (-), Moore (..), Skripalle (--).

4 CONCLUSION

The most promising model identified in this work is indeed the model proposed long ago by Faran. It is suitable for high density contrast systems, provides a rigorous description of the sonic behavior (then superior to available semiempirical models) and exhibits better numerical stability with respect to alternative detailed approaches, ECAH and HM.

REFERENCES

[1] Hipp, AK *et al.*, Particle Sizing in Colloidal Dispersions by Ultrasound. Model Calibration and Sensitivity Analysis, Langmuir 15, (1999) 2338–2345.

[2] Middleton, WD, Kurtz, AB, Ultrasound: The Requisites, (2003): Mosby.

[3] Atkinson, CM, Kytömaa, HK, Acoustic wave speed and attenuation in suspensions, Int. J. Multiph. Flow 18, (1992) 577–592.

[4] Atkinson, CM, Kytömaa, HK, Acoustic Properties of Solid-Liquid Mixtures and the Limits of Ultrasound Diagnostics—I: Experiments (Data Bank Contribution), J. Fluids Eng. 115, (1993) 665-675.

[5] Kytomäa, HK, Theory of sound propagation in suspensions: a guide to particle size and concentration characterization, Powder Technol. 82, (1995) 115–121.

[6] Dukhin, AS, Goetz, PJ, Acoustic Spectroscopy for Concentrated Polydisperse Colloids with High Density Contrast, Langmuir 12, (1996) 4987–4997.

[7] Hipp, AK, Acoustic Characterization of Particulate suspensions, (2001) ETH Zurich.

[8] Hipp, AK *et al.*, Acoustic Characterization of Concentrated Suspensions and Emulsions. 1. Model Analysis, Langmuir 18, (2002) 391–404.

[9] Faran, J, Sound Scattering by Solid Cylinders and Spheres, J. Acoust. Soc. Am. 23, (1951) 405–418.

[10] Epstein, P, Carhart, R, The Absorption of Sound in Suspensions and Emulsions.* I. Water Fog in Air, J. Acoust. Soc. Am. 239, (1953) 553-565.

[11] Allegra, J, Hawley, S, Attenuation of sound in suspensions and emulsions: Theory and experiments, J. Acoust. Soc. Am. (1972) 1545-1564.

[12] Hay, AE, Mercer, DG On the theory of sound scattering and viscous absorption in aqueous suspensions at medium and short wavelengths, J. Acoust. Soc. Am. 78, (1985) 1761-1771.

[13] Moore, SA, Monitoring flow and fluxes of suspended sediment in rivers using side-looking acoustic Doppler current profilers, (2006), Université de Grenoble.

[14] Skripalle, J *et al.*, Application of Multi-frequency Acoustics to Estimate Concentration of Suspended Sediments From Jurong Lake, 17th Intern. Seminar on Hydropower Plants, Singapore, (2012) 1–14.